Coordination Chemistry Reviews 255 (2011) 2693–2703

Contents lists available at ScienceDirect

Coordination Chemistry Reviews

journal homepage: www.elsevier.com/locate/ccr

Review

Photophysics of isomerizable Re(I) complexes: A theoretical analysis

Megumi Kayanuma[a], Chantal Daniel[a], Horst Köppel[b], Etienne Gindensperger[a,*]

[a] Laboratoire de Chimie Quantique, Institut de Chimie de Strasbourg, UMR7177CNRS-Université de Strasbourg, 4 Rue Blaise Pascal, CS 90032, F-67081 Strasbourg-Cedex, France
[b] Theoretische Chemie, Physikalisch-Chemisches Institut, Universität Heidelberg, Im Neuenheimer Feld 229, D-69120 Heidelberg, Germany

Contents

ARTICLE INFO

Article history:
Received 7 October 2010
Accepted 29 January 2011
Available online 11 March 2011

Keywords:
Rhenium
Carbonyl
Bipyridine
Isomerization
Excited state
Quantum chemistry

ABSTRACT

A theoretical exploration of the *trans–cis* photoisomerization of the 4-styrylpyridine (stpy) and 1,2-bis(4-pyridyl)ethylene (bpe) ligands L in $[Re(CO)_3(bpy)(L)]^+$ (bpy = 2,2′-bipyridine) complexes is performed on the basis of first-principles quantum chemical methods. The spin–orbit theoretical electronic absorption spectra are analysed and potential energy curves along a generalized coordinate combining several internal degrees of freedom involved in the isomerization process are determined and discussed. Our results are put in perspective with those obtained from recent picosecond/femtosecond time-resolved experiments. We provide a general mechanistic picture of the early steps of the process for this class of compounds. This contribution is the first theoretical "review" dedicated to the field of photoisomerizable Re(I) polypyridyl complexes.

1. Introduction

An extraordinary chemical flexibility combined with an exceptional tunable photoactivity makes the $[Re(L)(CO)_3(N,N)]^{n+}$ (N,N = polypyridines, α-diimine) complexes very attractive photosensitizers and probes, that may be used in biological systems, as well as in various materials such as polymers, molecular wires or liquid crystals [1–9]. The photophysical and photochemical properties of these molecules are governed by the nature of the π-acceptor and L axial ligands. Four types of electronic excited states characterize these complexes, namely metal-to-ligand-charge-transfer (MLCT), ligand-to-ligand charge transfer (LLCT), sigma-bond-to-ligand-charge-transfer (SBLCT) and intra-ligand (IL) states. Under UV–visible irradiation these molecules may be the seat of various competitive processes such as emission, electron/energy transfer, dissociation or isomerization. The quantum yields of these processes are controlled by the relative position of the low-lying excited states described above and by the dynamics of elementary processes such as intramolecular vibrational reorganization (IVR), intersystem crossing (ISC), internal conversion (IC) or solvation. Coordination of azobenzene and stilbene-like isomerizable ligands L to the Re(I) metal centre opens the route to new applications in

* Corresponding author.
E-mail address: egindensperger@unistra.fr (E. Gindensperger).

0010-8545/$ – see front matter © 2011 Elsevier B.V. All rights reserved.
doi:10.1016/j.ccr.2011.01.051

optical switches, photochemical memories or optically controlled molecular triggers [10]. The search for new compounds leading to highly efficient, ultra-fast and reversible photo-isomerization of the coordinated ligand L under visible light has attracted considerable activity in the last decade (see [11] and references therein). Upon alternate irradiation at different wavelengths a series of Re(I) tricarbonyl diimine complexes with various azo- and stilbene-containing ligands L undergo reversible *trans–cis* photoisomerization with modest quantum yields via ^{3}MLCT → ^{3}IL intra molecular energy transfer. As illustrated by a number of early experimental studies it has been established that the photoreactivity of 4-styrylpyridine complexes of Ru(II), Re(I) and W(0) is dominated by the photo-induced *trans–cis* isomerization of this ligand [12–14].

In order to understand and exploit the isomerization in this classes of molecules it is necessary to decipher the early relaxation processes in the low-lying singlet and triplet MLCT, LLCT, and IL excited states. The ultra-fast excited-state dynamics preceeding the ligand *trans–cis* isomerization in *fac*-[Re(Cl)(CO)$_3$(stpy)$_2$] and *fac*-[Re(stpy)(CO)$_3$(bpy)]$^+$ (with stpy = 4-styrylpyridine and bpy = 2,2′-bipyridine) has been investigated by means of time resolved spectroscopy [15]. [Re(diimine)(CO)$_3$(bpe)]$^+$ (with bpe = 1,2-bis(4-pyridyl)ethylene) display *trans* → *cis* bpe photoisomerization quantum yields on the order of 0.2–0.8 depending on the diimine ligand [16–18]. Due to the non-luminescence of *trans*-bpe complexes and despite of low luminescence quantum yields of the *cis*-bpe complexes (around 0.01) these molecules exhibit very pronounced photoswitchable luminescent properties [16]. More recently Iha et al. [17] reported a systematic experimental study of the absorption spectroscopy and photophysical behaviour of *fac*-[Re(CO)$_3$(Me$_4$phen)(trans-L)]$^+$ complexes (with Me$_4$phen = 3,4,7,8-tetramethyl-1,10-phenanthroline and L = stpy or bpe). In particular it was shown that the quantum yield of isomerization determined for the *trans*-bpe substituted complex is constant at all wavelengths of irradiation from 313 nm to 404 nm whereas the *trans*-stpy substituted complexes are characterized by quantum yields of isomerization which depend on the wavelength of irradiation. The quantum yields of isomerization are generally dependent on the polypyridyl ligand [18].

On the theoretical side, while several studies are devoted to free ligand isomerization [19–21], only a few studies are dedicated to the complicated processes occurring in transition metal complexes. A mechanism of *trans–cis* photoisomerization of the styrylpyridine ligand in [Re(CO)$_3$(bpy)(stpy)]$^+$ has been proposed on the basis of accurate *ab initio* calculations of the energy profiles of the low-lying MLCT and IL excited states as function of the C=C bond torsion angle [22]. However this one-dimensional picture, inspired by the simple model for stilbene-like molecules (Scheme 1), seems a little bit naive as illustrated by a number of recent experimental and theoretical studies reported on ultra-fast isomerization [23]. Indeed the commonly accepted mechanism of *trans–cis* photoisomerization is based on a very simple scheme describing the evolution of potential energy as a function of the torsion angle of the low-lying singlet states [24].

However a quantitative determination of the low-lying S_0, S_1 and S_2 electronic states and of the shapes of associated potential energy surfaces as a function of the most important degree of freedom is still lacking. For instance detailed analysis and interpretation of the vibronic structures of emission and absorption spectra of the two lowest ^1B_u states of stilbene requires accurate *ab initio* methods such as multi-state complete active space 2nd order perturbation theory (MS-CASPT2) calculations [19]. Moreover, as illustrated by a beautiful study reporting spectroscopic tracking of ultra-fast structural evolution in stilbene photoisomerization, the oversimplified one-dimensional isomerization coordinate model neglects global motions across the whole molecule [23]. This detailed Raman spectroscopic study combined with quantum chemical calculations

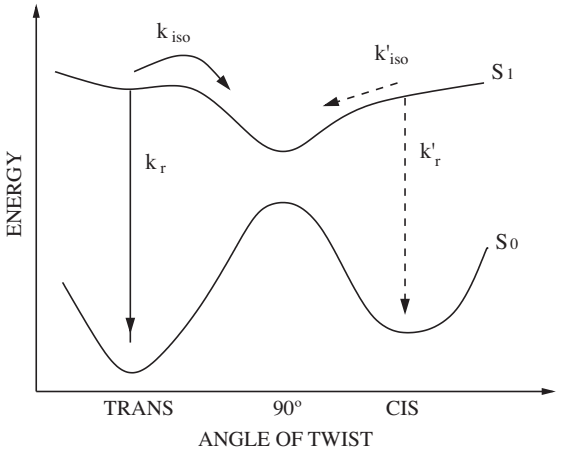

(courtesy of Waldeck [24]).

Scheme 1.

points to a continuous structural change during photoisomerization process with molecular rearrangements occurring on a time-scale comparable to nuclear vibrational periods (10 fs to ps). This is in contradiction with the oversimplified picture of a nearly flat S_1 potential energy profile along the ethylenic C–C bond torsion angle. A theoretical study reported by Martínez and coworkers [20] concludes that at least two nuclear reaction coordinates (twisting and pyramidalization) and three electronic states (S_0, S_1 and S_2) are necessary to interpret recent experiments performed on stilbene-like molecules. In a recent communication we have highlighted the key role of triplet states as well as spin–orbit and vibronic coupling providing a clear picture of the complicated mechanism of visible-light photoisomerization of Re(I) carbonyl-diimine complexes [25].

In the present work the UV–visible *trans–cis* photoisomerization of the 4-styrylpyridine (stpy) and 1,2-bis(4-pyridyl)ethylene (bpe) ligands L in [Re(CO)$_3$(bpy)(L)]$^+$ (bpy = 2,2′-bipyridine) complexes is investigated by means of first-principles quantum chemical methods. Curves of potential energy along a generalized coordinate combining several internal degrees of freedom primarily involved in the isomerization are determined and discussed. The influence of the elongation of the ethylenic carbon–carbon bond is included. The rich absorption spectrum in the UV–visible domain and the key role of spin–orbit and vibronic coupling in the early stage of the process are analysed. Our results are put in perspective with those obtained from experiments (^{1}H NMR, UV–visible absorption, Resonance Raman and infrared spectroscopies) [15–18].

2. Theoretical approach

The geometries of *trans* and *cis* isomers of [Re(CO)$_3$(bpy)(stpy)]$^+$ and [Re(CO)$_3$(bpy)(bpe)]$^+$ have been optimized by means of density functional theory (DFT) with the B3LYP functional with C_s symmetry for the *trans*(B) conformer and without symmetry constraints for all other *trans* and *cis* conformers, see Fig. 1.

The electronic structure of the ground and excited states of the *trans* and *cis* isomers was calculated at the State-Averaged Complete Active Space and Multi State 2nd Order Perturbation theory (SA-CASSCF/MS-CASPT2). Ten electrons (six 5d electrons and four π_{stpy} electrons) were correlated into eleven active orbitals. These include the five doubly occupied orbitals in the electronic ground state (three 5d and two π_{stpy}), and three 5d′, one π^*_{bpy}, and two π^*_{stpy} vacant orbitals for [Re(CO)$_3$(bpy)(stpy)]$^+$. For [Re(CO)$_3$(bpy)(bpe)]$^+$, we consider nine active orbitals including five doubly occupied orbitals in the electronic ground state

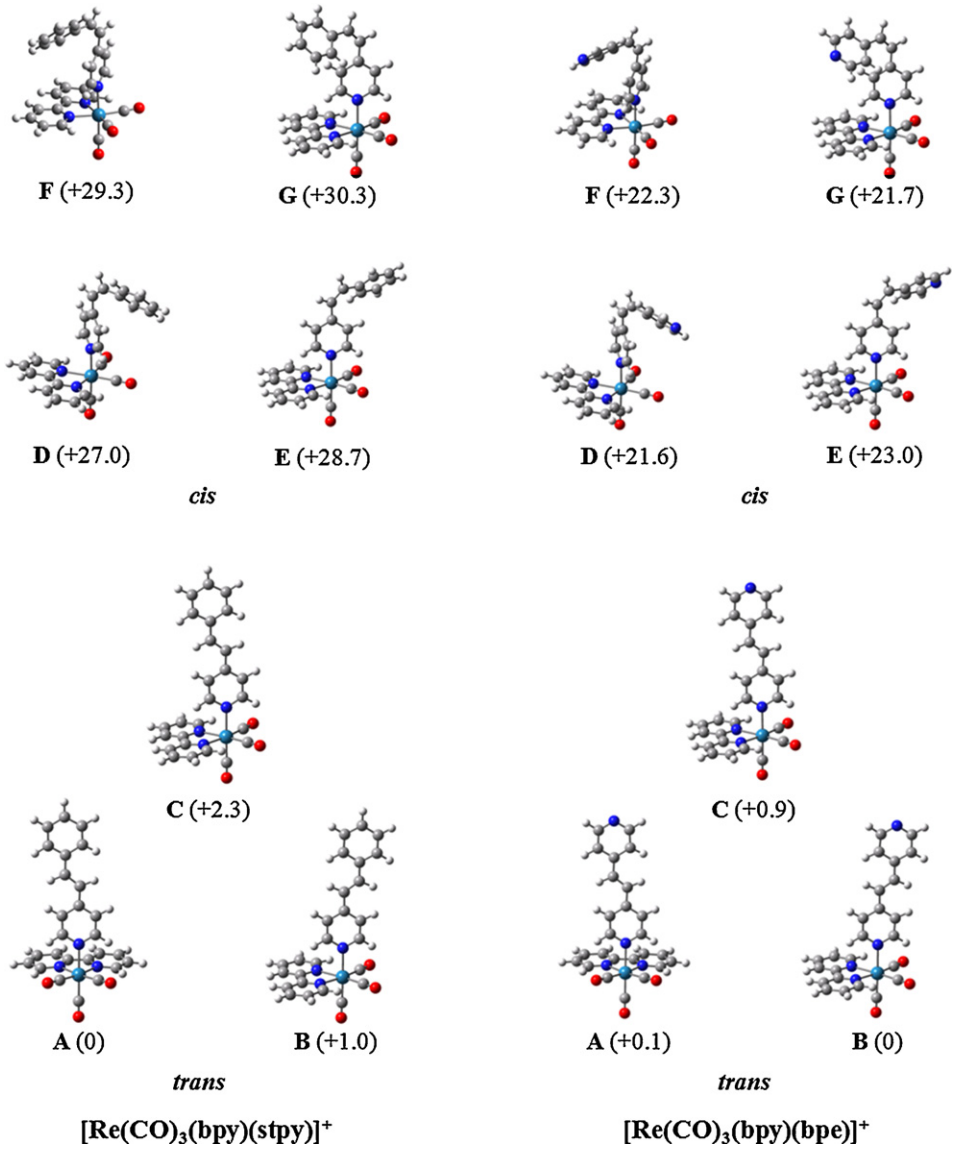

Fig. 1. Optimized structures of $[Re(CO)_3(bpy)(stpy)]^+$ and $[Re(CO)_3(bpy)(bpe)]^+$ complexes. Relative energies in kJ mol^{-1}.

(three 5d and two π_{bpe}), and two 5d′, one π^*_{bpy}, and one π^*_{bpe} vacant orbitals. A level shift correction of 0.2 hartree was applied to the MS-CASPT2 calculations to avoid intruder-state problems. The spin–orbit coupling is evaluated by the Restricted-Active-Space State-Interaction Spin–Orbit method (RASSI-SO).

The DFT optimized geometries of $[Re(CO)_3(bpy)(stpy)]^+$ were taken from Ref. [22], whereas $[Re(CO)_3(bpy)(bpe)]^+$ was optimized using relativistic pseudopotentials of Stuttgart and associated valence basis sets for rhenium atom [26] and Dunning double-ζ (DZP) basis sets for second-row and hydrogen atoms [27]. The excited state calculations of $[Re(CO)_3(bpy)(stpy)]^+$ and $[Re(CO)_3(bpy)(bpe)]^+$ at the CASSCF/MS-CASPT2 level were performed with the ANO-RCC (Atomic Natural Orbitals-relativistic correlation consistent) basis sets [28–30].

The potential energy curves (PECs) of the low-lying singlet and triplet states describing *trans*-$[Re(CO)_3(bpy)(stpy)]^+$ to *cis*-$[Re(CO)_3(bpy)(stpy)]^+$ isomerization process were calculated as a function of a generalized isomerization coordinate. The latter includes six internal degrees of freedom (depicted in Fig. 2) which are the driving coordinates of the isomerization process and are described in more detail in Section 3.2. All other geometrical parameters were frozen to those of the *trans* conformer. These calculations were performed with relativistic pseudopotentials of Stuttgart for the rhenium atom [26] and ANO-S basis set for other atoms [31]. Solvent effects are not included in the present study.

According to the size of the molecular system, the low symmetry of the process, and the high density of electronic states in the UV/vis domain of energy, other methods such as a systematic search for minimum energy paths or critical geometries from the Franck–Condon point are impracticable at present. Our *ab initio* calculations are at the limit of what can currently be done on these large molecules. The calculations reported in the present work were performed with the Gaussian 03 [32] and MOLCAS 7.2 [33] quantum chemistry softwares.

In Sections 5 and 6 we shall discuss the photoisomerization mechanism and relate it to the experimentally measured quantum yields. We do not calculate explicitly quantum yields, which would require to take into consideration the photons absorbed on the one hand, and the simulation of the dynamics on the excited states on the other hand, which is currently out of reach for our molecular systems. We rather discuss the isomerization probabilities which

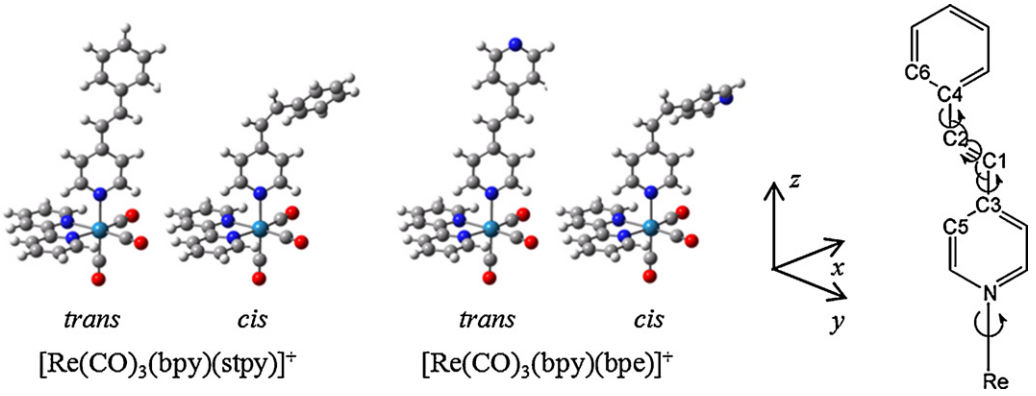

Fig. 2. *Trans* and *cis* structures of the two investigated molecules, i.e. $[Re(CO)_3(bpy)(stpy)]^+$ and $[Re(CO)_3(bpy)(bpe)]^+$ and description of the generalized isomerization coordinates for the potential energy curves.

can be inferred from the analysis of potential energy curves and coupling.

3. Geometries and isomerization pathways

In this section we discuss the optimized geometries of $[Re(CO)_3(bpy)(stpy)]^+$ and $[Re(CO)_3(bpy)(bpe)]^+$ complexes, and relate them to possible isomerization pathways. The former are used to define a generalized isomerization coordinate, along which the photoinduced process will be studied.

3.1. Geometries of trans and cis conformers

The various optimized geometries for $[Re(CO)_3(bpy)(stpy)]^+$ and $[Re(CO)_3(bpy)(bpe)]^+$ complexes are reported in Fig. 1, with the energies relative to the most stable structure given in kJ mol^{-1}. The results for $[Re(CO)_3(bpy)(stpy)]^+$ are those previously reported in Ref [22]. Three *trans* and four *cis* conformers are shown for each complex. The capital letters labelling the conformers follow the energetics of the $[Re(CO)_3(bpy)(stpy)]^+$ complex.

The two most stable *trans* conformers, (A) and (B), differ by the relative orientation of the isomerizable ligand with respect to what we shall call the principal plane of the molecule. This plane goes along the Re–N bond which links the stpy or bpe ligand to the transition metal and bisects the N–N bond of bpy. The isomerizable ligand is basically rotated by 90° between *trans*(A) and (B) structures. These structures are close in energy, with energy differences of 1 kJ mol^{-1} for $[Re(CO)_3(bpy)(stpy)]^+$ and only 0.1 kJ mol^{-1} for $[Re(CO)_3(bpy)(bpe)]^+$. It is the *trans*(B) structure of $[Re(CO)_3(bpy)(bpe)]^+$ which is slightly more stable, according to our results. In *trans*(A) and (B) conformers the isomerizable ligand is essentially planar. Experimental crystal structures for *trans*(A) conformers have been reported [11,16], and compare well with the theoretical results (see Ref. [22]). The *trans*(C) conformers, while resembling the *trans*(B) ones, exhibit isomerizable ligands which are rotated by 180°.

The four *cis* structures of each complex can also be distinguished by the orientation of the isomerizable ligand with respect to the principal molecular plane defined above. The pyridine group connecting to the Re atom lies either almost in this plane (*cis*(E) and (G) structures) or is almost perpendicular to it (*cis*(D) and (F) structures). Furthermore, for both types of structures the stpy or bpe ligand is oriented either towards the bpy ligand (F and G) or opposite to it (D and E). The combination of these two features leads to the four structures.

For $[Re(CO)_3(bpy)(bpe)]^+$, the energy differences between the *trans* and *cis* structures are smaller than those for $[Re(CO)_3(bpy)(stpy)]^+$ by roughly 7 kJ mol^{-1}, but all conformers of a given complex lie within 3 kJ mol^{-1}. While the *cis*(D) conformer is the most stable for both molecules, the other *cis* conformers are not energetically ordered in the same way. Interestingly, the main geometrical parameters are altogether very similar for both complexes for a given type of conformer, as can be inferred by comparing the left and right panels of Fig. 1.

3.2. Generalized isomerization coordinate

The orientation of the isomerizable ligand with respect to the principal molecular plane is of key importance to potentially define isomerization pathways. Indeed, it is probably not energetically favorable that the pyridine moiety connected to the rhenium atom undergoes a rotation of 90° during the photoinduced isomerization process. Thus isomerization of *trans*(A) conformers would preferably lead to *cis*(D) or (F), while isomerization of *trans*(B) or (C) conformers would lead to *cis*(E) or (G) complexes.

By analysing the geometries of the conformers, it is striking that the *trans*-to-*cis* isomerization cannot be properly described by a pure torsion of the ethylenic central C–C bound of stpy or bpe. This torsion is certainly the main geometrical parameter, but others are important as well. Indeed, one can clearly see that the upper ring of stpy or bpe is rotated. This additional molecular deformation is due to steric hindrance, and prevents the fold up of the ligand.

To conduct our analysis, we have thus identified the main geometrical deformations involved in the *trans*-to-*cis* isomerization. We have chosen to focus, in particular, on the isomerization from the *trans*(B) conformer to the *cis*(E) conformer, i.e. the conformer for which the isomerizable ligand lies initially in the principal molecular plane. The results reported in the following of this review will thus concern mainly this isomerization pathway. The conformers involved together with the generalized isomerization coordinate to be discussed now are reported in Fig. 2.

We have identified the six internal nuclear degrees of freedom which change most while comparing the *trans*(B) and *cis*(E) conformers. They define the generalized isomerization coordinate, which we shall call Q. One of them is of course the torsion of the ethylenic C–C bond. The others are rotations of the rings of the isomerizable ligand as well as angle opening around the ethylenic C–C bond. Finally, a small rotation (3°) of the whole ligand with respect to the main molecular plane has been included; this additional deformation turned out to be of minor relevance. The associated geometrical parameters for $[Re(CO)_3(bpy)(stpy)]^+$ are reported in Table 1, with the labelling corresponding to Fig. 2. Note that the additional rotations are by 25° and 31°, i.e. far from being negligible. Not to include them, and considering only pure torsion from the *trans* conformer would lead us very far from a realistic *cis* geom-

Table 1
Geometrical deformations defining the generalized isomerization coordinate Q for *trans*(B) to *cis*(E) isomerization of $[Re(CO)_3(bpy)(stpy)]^+$. See text for details, and Fig. 2 for the definition of the labels.

Angles/°	*trans*(B)	*cis*(E)
C3–C1–C2–C4	0	170.5
C1–C2–C4–C6	0	−31.4
C5–C3–C1–C2	180	205.0
C3–C1–C2	125.8	131.0
C1–C2–C4	127.4	131.6

etry, and the associated potential energy curves would lose much of their meaning.

To compute the isomerization potential energy curves along Q deformations, we have linearly interpolated between the *trans* and *cis* values. Defined in this way, Q does not correspond to deformations along a minimum energy path in the excited states of the molecule, neither to a minimum reaction path in the ground state. To compute such a minimum energy path, furthermore in a triplet state as we shall see, is computationally prohibitive, if manageable at all. Our generalized isomerization coordinate provides a simplified way of taking into account the main geometrical deformations, and in particular account for steric hindrance in such molecular systems. Q is used to compute the potential energy curves discussed in Sections 5 and 6. Having defined the isomerization coordinate, one needs to know which electronically excited states participate in the process according to the excitation wavelength used in experiments. The next section deals with the absorption spectroscopy of the $[Re(CO)_3(bpy)(stpy)]^+$ and $[Re(CO)_3(bpy)(bpe)]^+$ complexes.

4. UV–visible spectroscopies of $[Re(CO)_3(bpy)(stpy)]^+$ and $[Re(CO)_3(bpy)(bpe)]^+$

We have calculated the excited states of the $[Re(CO)_3(bpy)(stpy)]^+$ and $[Re(CO)_3(bpy)(bpe)]^+$ complexes using the method described in Section 2. For $[Re(CO)_3(bpy)(stpy)]^+$, the seven lowest singlets and six lowest triplets have been determined. For $[Re(CO)_3(bpy)(bpe)]^+$, the six lowest singlets and five lowest triplets have been determined. Calculations were performed with and without inclusion of the spin–orbit coupling.

4.1. *Trans(B) and cis(E)* $[Re(CO)_3(bpy)(bpe)]^+$

There are no experimental spectra for this complex, but there are for fac-$[Re(CO)_3(ph_2phen)(bpe)]^+$ (ph_2phen: 4,7-diphenyl-1,10-phenanthroline) [18], $[Re(CO)_3(Me_2bpy)(bpe)]^+$ (Me_2bpy: 4,7-dimethyl-bpy) [16], and $[Re(CO)_3(phen)(bpe)]^+$ (phen: 1,10-phenantroline) [34,35]. The spectra of Ref. [18], reproduced in Fig. 3, are characterized by a strong absorption band at 300 nm attributed to a ^{1}IL state, corresponding to a $\pi\pi^*_{bpe}$ excitation, which possesses a shoulder which extends to low energies up to 450 nm, due to MLCT states. The *cis* isomer absorbs less than the *trans* around 300 nm.

Our spin-free results for $[Re(CO)_3(bpy)(bpe)]^+$ are summarized in Table 2. For the *trans* conformer, the lowest excited state is a ^{3}IL state corresponding to a $\pi\pi^*$ excitation localized on the bpe ligand, at 24 700 cm^{-1}. Slightly above is a bench of singlet and triplet MLCT states from the 5d orbitals of the Re(I) to a π^* orbital of the bpy ligand. The triplet MLCT states are below their corresponding singlets by 400–1000 cm^{-1}. These six MLCT states are close in energy and lie in an energy range of 4000 cm^{-1}. At an energy of 33 750 cm^{-1} is the strongly absorbing ^{1}IL state, corresponding to the $\pi\pi^*_{bpe}$ transition. Above 35 000 cm^{-1} we have additional triplet and singlet IL_{bpe} states. There is no $MLCT_{bpe}$ state in the investigated energy domain; these states lie at higher energies. The results for the *cis* conformer are rather similar, with one important difference: ^{3}MLCT states are below the ^{3}IL state at this geometry. This will have an important impact on the luminescence properties of the complexes, as we shall discuss later. Indeed, the energies of the ^{3}MLCT states are slightly decreased compared to the *trans* values, but it is mainly the ^{3}IL which goes up, at an energy of 28 600 cm^{-1}, explaining the partial reordering of the electronic states.

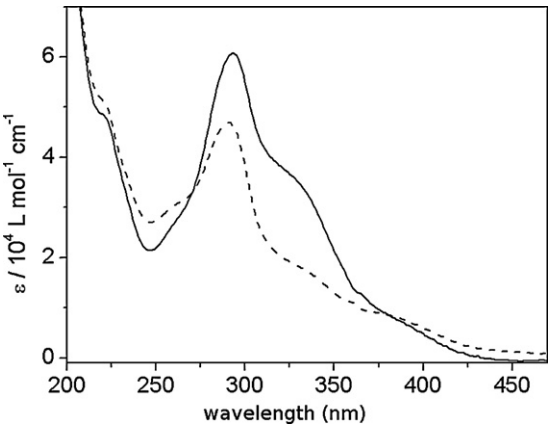

Fig. 3. Molar absorptivities of fac-$[Re(CO)_3(ph_2phen)(cis\text{-}bpe)]^+$ (- - -) (ph_2phen: 4,7-diphenyl-1,10-phenanthroline) in comparison with fac-$[Re(CO)_3(ph_2phen)(trans\text{-}bpe)]^+$ (—) (by courtesy of the author, Ref. [18]).

The calculated spin-free absorption spectra for both *trans* and *cis* isomers are shown in Fig. 4a. These spectra have been obtained by convolution of the line spectra by Gaussians, to account for the broadening of the spectral lines. The theoretical spectra agree well with the experimental one shown in Fig. 3 as far as the position of the maximum absorption band is concerned. The maximum is however slightly shifted for the *cis* isomer towards higher energies, as compared with the experimental spectrum of Ref. [18]. Interestingly, such a shift has been observed by Gray and coworkers [16] with Me_2bpy instead of the ph_2phen ligand, and our values for transition energies with the bpy ligand are in good agreement with their values. Thus, these ligands have also an impact, even if moderate, on the energetics of the IL_{bpe} states.

The influence of bpy, phen, Me_2bpy or ph_2phen ligands onto the IL states of the isomerizable one can easily be explained by the lack of any symmetry in the complex. Thus, all electronic states can interact, and interact differently depending on the particular molecular geometry.

The shoulder of the spectrum does not extend sufficiently to low energies. Indeed, isomerization occurs after irradiation around 400 nm [16–18], and no state absorbs in this energy domain according to the results reported in Table 2. Involving 5d orbitals of the rhenium, MLCT states are likely subject to spin–orbit coupling. We have thus accordingly calculated the spin–orbit transitions. The

Table 2
CASSCF/CASPT2 spin-free transition energies [cm^{-1}] and oscillator strength [*f*] of *trans*- and *cis*-$[Re(CO)_3(bpy)(bpe)]^+$ conformers.

$[Re(CO)_3(bpy)(bpe)]^+$		*trans*(B)		*cis*(E)	
State		Energy/cm^{-1}	*f*	Energy/cm^{-1}	*f*
a^3IL	$\pi_{bpe} \rightarrow \pi^*_{bpe}$	24 700		28 610	
a^3MLCT	$5d_{xz} \rightarrow \pi^*_{bpy}$	28 330		28 550	
a^1MLCT	$5d_{xz} \rightarrow \pi^*_{bpy}$	28 980	0.028	28 960	0.029
b^3MLCT	$5d_{yz} \rightarrow \pi^*_{bpy}$	29 810		27 120	
b^1MLCT	$5d_{yz} \rightarrow \pi^*_{bpy}$	30 960	0.214	30 970	0.212
c^3MLCT	$5d_{xy} \rightarrow \pi^*_{bpy}$	32 030		30 690	
c^1MLCT	$5d_{xy} \rightarrow \pi^*_{bpy}$	32 400	0.035	32 390	0.033
a^1IL	$\pi_{bpe} \rightarrow \pi^*_{bpe}$	33 750	1.212	34 570	0.691
b^3IL	$\pi_{bpe} \rightarrow \pi^*_{bpe}$	35 660		34 360	
b^1IL	$\pi_{bpe} \rightarrow \pi^*_{bpe}$	37 140	0.182	38 630	0.166

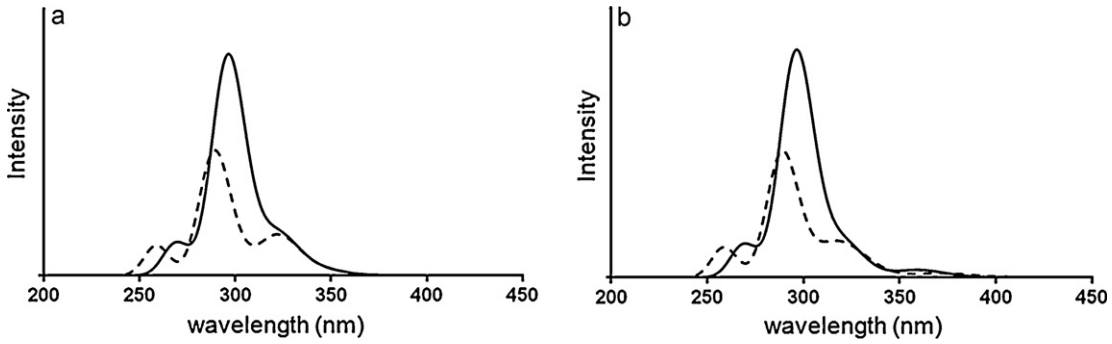

Fig. 4. Calculated spin-free (a) and spin–orbit (b) absorption spectra of *trans* (solid line) and *cis* (dashed line) structures of $[Re(CO)_3(bpy)(bpe)]^+$. The calculated spectrum is obtained by convoluting the theoretical line spectrum by Gaussians of 1000 cm^{-1} FWHM.

results are presented in Table 3, where the mixing of singlets and triplets are given. Let us focus again on the *trans* conformer. We clearly see that the a^3IL is not affected by spin–orbit coupling, and the triplet remains pure (triply degenerate). This transition is entirely localized on the bpe ligand and does not involve the transition metal, and behaves as in the free organic ligand.

In contrast, the spin–orbit coupling has an important effect on MLCT states. Indeed, calculated coupling constants are as high as 700–900 cm^{-1}, close to the atomic Re value. It can be seen that triplet states are mixed between themselves, but also and more importantly with singlet states, thus sharing some oscillator strength. Indeed, the lowest absorbing state is of triplet nature by 81%, but the 9% singlet contribution suffices to provide an oscillator strength of 0.023. It is small, but the absorption around 400 nm proceeds in the tail of the absorption spectrum, see Fig. 3. Our calculated energy is decreased as compared to the spin-free lowest absorbing state, but is still more than 2500 cm^{-1} too high (400 nm is equivalent to 25 000 cm^{-1}). The fact that the MLCT states are too high in energy by a few thousand wavenumbers will also occur for the $[Re(CO)_3(bpy)(stpy)]^+$ complex, and is probably due to the neglect of solvent effects and contributions of non purely vertical transitions as we shall discuss in more detail later.

In Fig. 4b we show the theoretical absorption spectra obtained by inclusion of the spin–orbit coupling. We see clearly that the shoulder extends to lower energies, as compared to Fig. 4a for the spin-free case. The strong absorption band is not affected by the spin orbit coupling as it corresponds to a ^{1}IL state. The spin–orbit coupling is not only a key ingredient for the absorption in the tail of the spectrum, it will also allow for transitions between the various electronic states during the photoisomerization process in itself, see Section 5.

The results including spin–orbit coupling show that the a^3IL state is not the lowest excited states for the *cis* conformer. Four spin–orbit states lie below, and two of them possess non-negligible oscillator strength. In the $[Re(CO)_3(Me_2bpy)(bpe)]^+$ complex studied by Gray and coworkers [16], emission of the *cis* conformer was reported, while the *trans* does not emit. It is thus a molecular switch. Our results are fully in line with this finding. Since the a^3IL is not the lowest excited state in the *cis* conformation, electronic population is transferred to the low lying MLCT states, from which the complex can emit. Gray reported yellow emission, around 18 000 cm^{-1}. Our MLCT states at the *cis* ground state equilibrium geometry are higher in energy, showing that relaxation processes in the MLCT states occur, lowering their energy. The emission is rather weak [16], as explained by the small calculated oscillator strength.

4.2. *Trans(B) and cis(E) $[Re(CO)_3(bpy)(stpy)]^+$*

A similar analysis has been conducted for the *trans*(B) and *cis*(E) $[Re(CO)_3(bpy)(stpy)]^+$ complexes. Here, an experimental absorption spectrum is available for the *trans* moiety [15]. Our spin-free results are reported in Table 4.

Table 3
CASSCF/CASPT2 spin–orbit transition energies [cm^{-1}] and oscillator strength [*f*] of *trans*- and *cis*-$[Re(CO)_3(bpy)(bpe)]^+$ conformers.

$[Re(CO)_3(bpy)(bpe)]^+$	*trans*(B)		*cis*(E)		
Spin-free state and weight	Energy/cm^{-1}	*f*	Spin-free state and weight	Energy/cm^{-1}	*f*
a^1A (100%)			a^1A (100%)		
a^3IL (100%)	24 700		a^3MLCT (71%), b^3MLCT (21%)	26 230	
a^3IL (100%)	24 700		a^3MLCT (74%), b^3MLCT (21%)	26 360	
a^3IL (100%)	24 700		a^3MLCT (86%), b^1MLCT (7%)	26 560	0.012
a^3MLCT (71%), b^3MLCT (21%)	27 450		b^3MLCT (50%), a^3MLCT (37%)	27 300	0.010
a^3MLCT (72%), b^3MLCT (21%)	27 480		a^3IL (100%)	28 610	
a^3MLCT (81%), b^1MLCT (9%)	27 650	0.023	a^3IL (100%)	28 610	
a^1MLCT (61%), b^3MLCT (29%)	27 900	0.017	a^3IL (100%)	28 610	
b^3MLCT (73%), a^3MLCT (25%)	30 260		b^3MLCT (72%), a^3MLCT (26%)	29 020	
b^3MLCT (74%), a^3MLCT (25%)	30 270		b^3MLCT (76%), a^3MLCT (23%)	29 040	
b^3MLCT (66%), a^1MLCT (34%)	30 430	0.010	a^1MLCT (51%), b^3MLCT (47%)	29 680	0.015
b^1MLCT (73%), a^3MLCT (17%)	31 130	0.166	c^3MLCT (52%), b^1MLCT (34%)	30 590	0.076
c^3MLCT (90%)	32 470		c^3MLCT (90%)	31 130	
c^3MLCT (90%)	32 490		c^3MLCT (85%)	31 230	
c^3MLCT (78%), b^1MLCT (16%)	32 560	0.026	b^1MLCT (60%), c^3MLCT (40%)	31 660	0.127
c^1MLCT (89%)	32 800	0.042	c^1MLCT (95%)	32 670	0.029
a^1IL (100%)	33 760	1.204	b^3IL (100%)	34 360	
b^3IL (100%)	35 660		b^3IL (100%)	34 360	
b^3IL (100%)	35 660		b^3IL (100%)	34 360	
b^3IL (100%)	35 660		a^1IL (100%)	34 580	0.690
b^1IL (100%)	37 140	0.182	b^1IL (100%)	38 630	0.166

Table 4
CASSCF/CASPT2 spin-free transition energies [cm^{-1}] and oscillator strength [*f*] of *trans*- and *cis*-$[Re(CO)_3(bpy)(stpy)]^+$ conformers.

$[Re(CO)_3(bpy)(stpy)]^+$		*trans*(B)		*cis*(E)	
State		Energy/cm^{-1}	*f*	Energy/cm^{-1}	*f*
a^3IL	$\pi_{stpy} \rightarrow \pi^*_{stpy}$	22 900		24 840	
a^3MLCT	$5d_{xz} \rightarrow \pi^*_{bpy}$ (70%)	27 870		27 680	
/LLCT	$\pi_{stpy} \rightarrow \pi^*_{bpy}$ (9%)				
a^1MLCT	$5d_{xz} \rightarrow \pi^*_{bpy}$ (60%)	28 380	0.023	28 340	0.022
/LLCT	$\pi_{stpy} \rightarrow \pi^*_{bpy}$ (20%)				
b^3MLCT	$5d_{yz} \rightarrow \pi^*_{bpy}$	29 260		29 080	
a^1IL	$\pi_{stpy} \rightarrow \pi^*_{stpy}$	30 100	1.368	30 540	0.824
b^1MLCT	$5d_{yz} \rightarrow \pi^*_{bpy}$	30 600	0.204	30 180	0.209
c^3MLCT	$5d_{xy} \rightarrow \pi^*_{bpy}$	31 900		30 720	
c^1MLCT	$5d_{xy} \rightarrow \pi^*_{bpy}$	32 350	0.016	31 310	0.019
a^3LLCT	$\pi_{stpy} \rightarrow \pi^*_{bpy}$ (77%)	34 530		34 630	
/MLCT	$5d_{xz} \rightarrow \pi^*_{bpy}$ (8%)				
a^1LLCT	$\pi_{stpy} \rightarrow \pi^*_{bpy}$ (60%)	35 450	0.003	35 280	0.004
/MLCT	$5d_{xz} \rightarrow \pi^*_{bpy}$ (20%)				
b^3IL	$\pi_{stpy} \rightarrow \pi^*_{stpy}$	36 350		35 060	
b^1IL	$\pi_{stpy} \rightarrow \pi^*_{stpy}$	37 130	0.104	37 300	0.097

By comparing to the results for $[Re(CO)_3(bpy)(bpe)]^+$, several important differences arise. The first is that we have additional contributions from a Ligand-to-Ligand Charge Transfer state (LLCT) involving a $\pi_{stpy} \rightarrow \pi^*_{bpy}$ excitation. This state is strongly mixed with the lowest $MLCT_{bpy}$ state for the singlet as well as the corresponding triplet. Such LLCT state also exists in $[Re(CO)_3(bpy)(bpe)]^+$ at higher energies (not discussed).

The second difference is that the a^3IL as well as the a^1IL states are lower in energy than their equivalent in $[Re(CO)_3(bpy)(bpe)]^+$ by 2000–3000 cm^{-1}, while the energy of the MLCT states is roughly the same. As a consequence, the a^3IL state remains the lowest excited state in the *cis* isomer.

The theoretical spin–orbit spectrum for *trans* $[Re(CO)_3(bpy)(stpy)]^+$ is reported in Fig. 5 together with the experimental one of Vlček and coworkers [15]. The calculated values are provided in Table 5. The results for the *cis* conformer are similar to those of the *trans* (not shown).

The maximum absorption band corresponding to the a^1IL state is located at 332 nm, agreeing very well with the experimental results [15]. However, a spike in the experimental spectrum is present at 320 nm. It corresponds to a $^1IL_{bpy}$ state localized on the bpy ligand [15]. This electronic state is not included in our calculation for technical reasons: we cannot properly describe both the $^1IL_{bpy}$ and $^1IL_{stpy}$ states, this would require additional orbitals to be included in the calculations. However, this $^1IL_{bpy}$ state lies quite high in energy, and is unlikely to participate in the isomerization process. It is thus excluded from our calculations. Note that a corresponding $^1IL_{diimine}$ state should also appear in the $[Re(CO)_3(ph_2phen)(bpe)]^+$ complex and is probably partly responsible for the absorption around 325 nm [18].

Inclusion of the spin–orbit coupling mixes the singlet and triplet MLCT states and decreases their energy, while the IL states are not affected, like in the free organic ligand.

By comparing the results for the two investigated molecules, one clearly sees that replacing the bpe ligand by the stpy has an important impact. The energetics of the IL states, both singlet and triplet, are affected. In the $[Re(CO)_3(bpy)(bpe)]^+$ complex, the ^{3}IL is close in energy to the MLCT states, and even is above some of them in the *cis* conformer. The ^{1}IL lies above all the low lying MLCT states. In contrast, with the stpy ligand, the ^{3}IL state is lower in energy, being roughly half an eV below the MLCT states. The ^{1}IL state is completely embedded in the bench of MLCT states. These results are in accordance with experimental data [15–18].

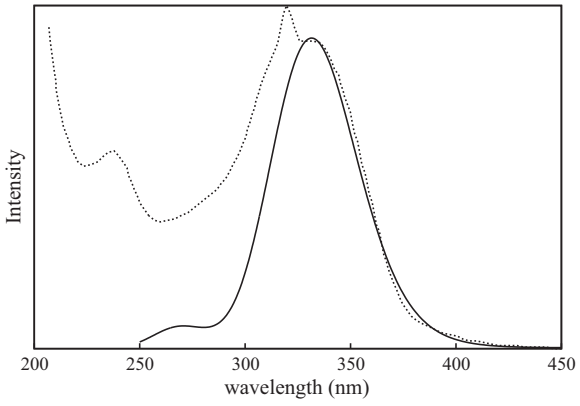

Fig. 5. Calculated absorption spectrum (spin–orbit) of *trans*(B) $[Re(CO)_3(bpy)(stpy)]^+$ (solid line) and experimental spectrum (dotted line) from Ref. [15]. The calculated spectrum is obtained by convoluting the theoretical line spectrum by Gaussians of 1000 cm^{-1} FWHM.

Table 5
CASSCF/CASPT2 spin–orbit transition energies [cm^{-1}] and oscillator strength [*f*] of *trans*-$[Re(CO)_3(bpy)(stpy)]^+$ conformer.

$[Re(CO)_3(bpy)(stpy)]^+$	*trans*(B)	
Spin-free state and weight	Energy/cm^{-1}	*f*
a^1A (100%)		
a^3IL (100%)	22 900	
a^3IL (100%)	22 900	
a^3IL (100%)	22 900	
a^3MLCT/LLCT (71%), b^3MLCT (21%)	27 040	
a^3MLCT/LLCT (72%), b^3MLCT (21%)	27 070	
a^3MLCT/LLCT (83%), b^1MLCT (10%)	27 260	0.021
a^1MLCT/LLCT (63%), b^3MLCT (28%)	27 410	0.014
b^3MLCT (73%), a^3MLCT/LLCT (25%)	29 700	
b^3MLCT (75%), a^3MLCT/LLCT (25%)	29 700	
b^3MLCT (66%), a^1MLCT/LLCT (33%)	29 810	0.008
a^1IL (100%)	30 090	1.370
b^1MLCT (76%), a^3MLCT/LLCT (15%)	30 730	0.157
c^3MLCT (90%)	32 270	
c^3MLCT (92%)	32 270	
c^3MLCT (83%), b^1MLCT (14%)	32 360	0.022
c^1MLCT (91%)	32 670	0.017
a^3LLCT/MLCT (100%)	34 530	
a^3LLCT/MLCT (100%)	34 530	
a^3LLCT/MLCT (100%)	34 530	
a^1LLCT/MLCT (100%)	35 490	0.003
b^3IL (100%)	36 370	
b^3IL (100%)	36 370	
b^3IL (100%)	36 370	
b^1IL (100%)	37 130	0.104

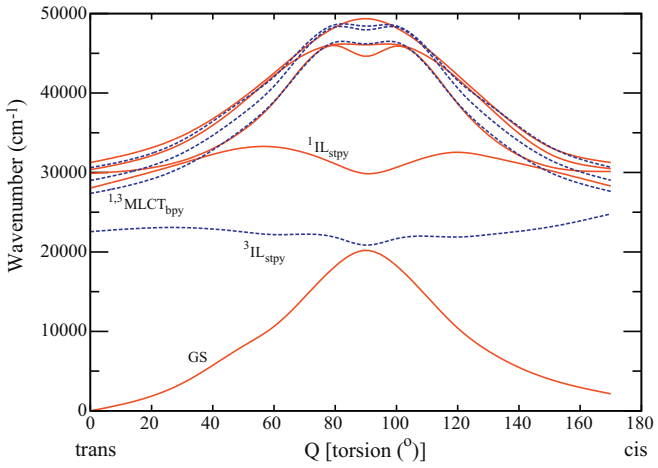

Fig. 6. Adiabatic potential energy curves along Q deformation, as a function of the torsion angle of the ethylenic C–C bond. The spin-free singlet states (red, solid line) and triplet states (blue, dashed line) are shown. Note that, according to Table 4, the ^{1}IL$_{stpy}$ state is the second singlet excited state at the trans geometry. It crosses a ^{1}MLCT state around 35°.

We have also conducted an analysis of the theoretical absorption spectrum of the *trans*(A) conformer of $[Re(CO)_3(bpy)(stpy)]^+$. The results, not shown, are very close to those of the *trans*(B) one discussed so far. Indeed, the MLCT states involving the transition metal and the bpy ligand on one hand, and the IL states localized on the stpy on the other hand, are quite little affected by the rotation of the latter by 90° with respect to the principal molecular plane. The LLCT contributions change however, but not as much as we could have expected.

5. Potential energy curves and photoisomerization mechanisms

In this section, we describe in some detail the photoisomerization mechanisms occuring in the $[Re(CO)_3(bpy)(stpy)]^+$ complex, based on the use of the generalized isomerization coordinate Q, and exploiting the results presented in Section 4.

5.1. Potential energy curves of photoisomerization

To study the photoisomerization of the $[Re(CO)_3(bpy)(stpy)]^+$ complex, we have performed ab initio calculations along the isomerization pathway described by the generalized coordinate Q, see Section 3.2. The spin-free potential energy curves for the five lowest singlet and four lowest triplet states are shown in Fig. 6. To show the spin–orbit curves would have complicated the figure while providing only little additional information.

We clearly see that the ground state exhibits the usual transition-state behaviour for isomerization, with the maximum of the barrier at the perpendicular geometry (90°). The ground state energy in the *cis* isomer is 2000 cm^{-1} higher than that in the *trans* isomer. The overall shape of the ground-state potential energy curve is rather symmetric. Two sets of excited states potential energy curves which behave differently are put in evidence by our calculations. The first group is associated to the low-lying MLCT states. Their shapes follow that of the ground state potential. This is logical, since isomerization along Q involves geometrical changes only in the stpy ligand, and the energy gap between MLCT states and the ground state is almost invariant under isomerization. We can observe however that around the perpendicular geometry the shape of the potential energy curves of the MLCT states are altered. This is due to couplings with higher lying states, and is not discussed further here.

The second set of potential energy curves is associated to the IL states. The shape of the ^{1}IL state presents two energy barriers, around 60° and 120°, and a minimum at the perpendicular geometry. Note that, according to Table 4, the ^{1}IL state is the second singlet excited state at the *trans* and *cis* geometries. It crosses the lower lying ^{1}MLCT state around 35° and 145°, and becomes the lowest singlet excited state in between. This crossing, i.e. a conical intersection [36], occurs before the barrier at 60°, and at a lower energy; it will have an impact in the isomerization process upon UV-light irradiation, as we shall discuss later.

The ^{3}IL state is characterized by a rather flat shape potential, with a shallow minimum at the equilibrium geometry. It is the *only* electronically excited state below 25 000 cm^{-1}, and the isomerization process occuring after 400 nm irradiation must proceed via this state. The ^{1}IL state is too high in energy, and the MLCT states posses a large barrier to isomerization. The ^{3}IL state does not absorb, the low energy absorption proceeds in the low lying MLCT states, as found experimentally [15–18]. This gives rise to a multistep process for the isomerization, as discussed in the following. At shorter excitation wavelength, the ^{1}IL can be excited as well, and isomerization potentially occurs also in this state.

On the basis of our calculations, and the data available from experiments, in particular those from the femtosecond/picosecond spectroscopies of Vlček and coworkers [15] which provide time scales, we shall analyse the various steps of the photoisomerization process in the $[Re(CO)_3(bpy)(stpy)]^+$ complex. We use a spin-free vocabulary for the subsequent discussion, and start with the process after 400 nm irradiation.

5.2. Photoisomerization mechanism upon visible irradiation

After absorption at 400 nm, only the lower lying ^{1}MLCT state is populated. Then a very fast intersystem crossing (ISC) to the corresponding ^{3}MLCT state follows. A time scale of only 200 fs has been reported [15], largely explained by the fact that the states are almost degenerate in this region, as already discussed (see also Tables 4 and 5). Alongside, the spin–orbit coupling among these states is very large (700–900 cm^{-1}) leading to an ultrafast ISC. According to the spin–orbit absorption spectrum, see Table 5, a direct excitation of a "triplet" state also occurs (triplet component greater than 80%). Consequently, the ^{3}MLCT state is populated either "directly" or via the corresponding ^{1}MLCT state.

The second step of the photoisomerization process is an intramolecular energy transfer from the ^{3}MLCT to the ^{3}IL state. This step has been experimentally given a time-scale of 3.5 ps. Our energy gap of 4200 cm^{-1} is quite large, half an eV.

This energy gap could be reduced by the influence of other nuclear degrees of freedom. Indeed, a shortening of the central C–C bond length of bpy, and of the Re–N distances in the bpy ligand reduces this gap to roughly 3000 cm^{-1}. The MLCT$_{bpy}$ states are stabilized, while the IL$_{stpy}$ are unaffected. This has two consequences. (i) Absorption can take place at a lower energies than the calculated Franck–Condon transitions. (ii) There is enough time for a relaxation in the ^{3}MLCT state during the 3.5 ps. Nevertheless, the presence of this gap explains the larger timescale of this step. The ^{3}IL state is formed vibrationally hot.

A Dexter type process has been invoked [15] to explain this triplet–triplet transition. Since we consider here directly the entire molecule, and not two fragments or parts which can further interact, exchange interactions are directly included in our calculations. This intramolecular energy transfer does not appear to be driven by a Dexter mechanism. Rather, we would like to emphasize that within a given molecular system, vibronic coupling do occur also in the triplet manifold. This coupling may lead to very fast internal conversion. As a consequence, during this step electronic pop-

ulation is transferred from the ligand which participates in the absorption (bpy) to the one which isomerizes.

Once in the ^{3}IL state, isomerization may occur, as can be seen in Fig. 6. A perpendicular intermediate has been postulated according to experiments, which is obtained after 12 ps [15]. Our curve supports a quite delocalized nature of the ^{3}IL state, due to the flatness of the curve. However, nuclear relaxation will play a role, and other degrees of freedom than those included here will affect the energy of the ^{3}IL state. Our curve suggests a quantum yield of roughly 0.5, close to the experimental finding of 0.4 [15,17,18].

The last step of the process is the transition to the *cis* isomer or back to the *trans* one in the ground state. This proceeds very slowly, within 17 ns [15]. On our curves, Fig. 6, there is a small energy gap between the ^{3}IL and the ground state at the perpendicular geometry. Increasing the ethylenic C–C bond distance decreases this gap, and the two states become exactly degenerate. Around the perpendicular geometry, the C–C bond is closer to a single bond than to a double bond. Even if degenerate, our computed spin–orbit coupling between the ground and ^{3}IL states at the perpendicular geometry is nearly zero. This is a spin-forbidden transition, explaining the long life-time of the triplet state. This contrasts drastically with the strong spin–orbit coupling in the Re-bpy part. When going from the $MLCT_{bpy}$ states to the $^3IL_{stpy}$ state, the spin–orbit coupling switches from the quasi atomic value of the transition-metal centre to zero. This feature may have interesting consequences on the – photoinduced – magnetic properties of such complexes.

5.3. Photoisomerization mechanism upon UV irradiation

Under excitation at higher energies (365 nm and 334 or 313 nm), an increase of the quantum yields is typically observed [15,17,18]. One of the options is that the ^{1}IL pathway is activated. To that end, we have tried to find a reduced energy gap between this state and the ground state at the perpendicular geometry, by means of the so-called pyramidalization of the ligand, as has been done for free stilbene [20]. It appears that such a deformation does not decrease the gap. Other deformations will certainly do, but this is left for future work. However, there is already a second, alternative option. As can clearly be seen in Fig. 6 and already discussed, the ^{1}IL state crosses the ^{1}MLCT around 35°. This corresponds to a true crossing if the ethylenic C–C bond length is increased. The crossing, or conical intersection, is located before the barrier in the ^{1}IL state upon deformation along Q. Thus, after excitation in this energy range, population will be very efficiently transferred to the ^{1}MLCT state, and with excess energy compared to the direct absorption in this state. The various steps described so far will be followed again, but with additional energy. Part of this energy will be quickly dissipated in the solvent and local environment, but can still explain an increase of the quantum yield due to the long life-time of the ^{3}IL state. Absorption in the ^{1}IL state will thus enhance the activation of the "triplet pathway". The two pathways are summarized in Fig. 7, which shows the potential energy surfaces of the singlet and triplet IL states together with the ground state as a function of Q and of the elongation of the ethylenic C–C bond.

The location of the conical intersetion(s) and the energy gap between the MLCT and the IL states will strongly depend on both ligands. Complexation to a transition metal acts as a triplet sensitizer in *two* different ways. (i) The usual one, i.e. excitation to the low-lying MLCT states leads to a fast and efficient population of the ^{3}IL state. But, also, (ii) the MLCT states, by crossing the ^{1}IL surface, act as to mediate population transfer from this singlet IL state to the corresponding triplet.

Note also that around 320 nm a IL_{bpy} state also absorbs in the $[Re(CO)_3(bpy)(stpy)]^+$ complex [15]. This state is not included in our calculations (see Section 2). The presence of this state will increase the absorption of the molecule below 320 nm. This will lead to an

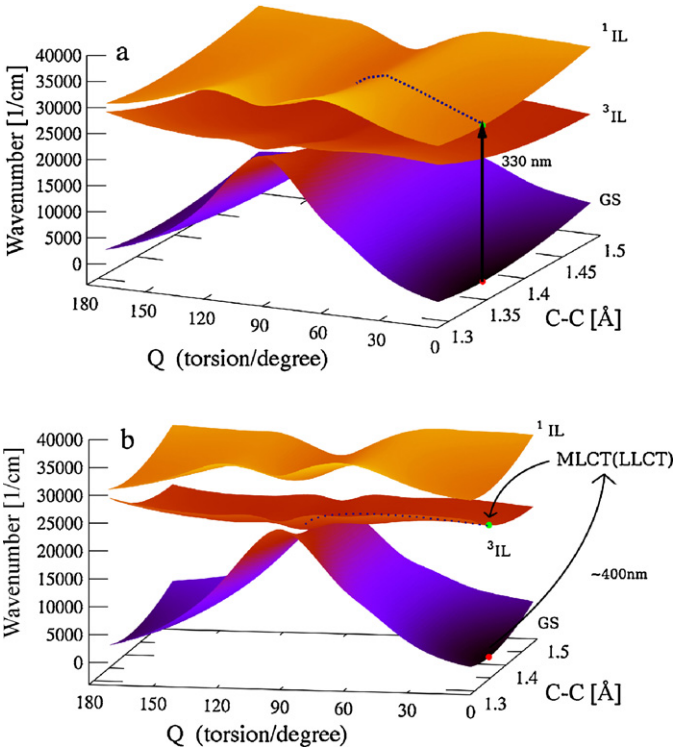

Fig. 7. Two-dimensional potential energy surfaces for the ground, singlet and triplet IL states, showing the mechanism of isomerization at 400 and 330 nm in $[Re(CO)_3(bpy)(stpy)]^+$.

increase of the population of the $^1Il_{stpy}$ state by internal conversion, and may help to overcome the barrier around 60° due to the excess energy. The shape of the potential energy curve of the IL_{bpy} state will be comparable to that of the $MLCT_{bpy}$ states. Indeed, deformations along Q will have little impact on the IL_{bpy} state, which will roughly follow the shape of the ground-state potential energy curve, as is the case for the $MLCT_{bpy}$ states.

Several experimental studies are available for which the ligands have been substituted [15–18], and the quantum yields of isomerization are strongly affected. We shall discuss some of them in the following concluding remarks.

6. Concluding remarks

The mechanism of UV–visible light photoinduced isomerization processes of stilbene-like ligands L coordinated to rhenium(I) centres has been investigated by accurate *ab initio* calculations of the *trans*- and *cis*-isomeric electronic structures in the ground and excited states, and the determination of potential energy profiles taking into account several internal degrees of freedom. The electronic absorption spectra, including spin–orbit corrections, of $[Re(CO)_3(bpy)(L)]^+$ (L = stpy or bpe) are characterized by two regions of interest with a strong band located around 310 or 330 nm (^1IL_L transition) and a tail around 400 nm ($^1MLCT_{bpy}$ transitions) in agreement with experimental features. The $^1MLCT_{bpy}$ and $^3MLCT_{bpy}$ states are almost degenerate in the Franck–Condon region and are coupled by large spin–orbit coupling (700–900 cm^{-1}) leading to very fast and efficient intersystem crossing (ISC) with an experimental time scale of about 200 fs. In $[Re(CO)_3(bpy)(stpy)]^+$ the ^3IL_L state is well separated of this set of MLCT states by little less than 0.5 eV in accord with an experimental intramolecular energy transfer time-scale of 3.5 ps. For $[Re(CO)_3(bpy)(bpe)]^+$ the ^3IL_L is closer in energy to the MLCT states, and the time scale of energy transfer should be reduced.

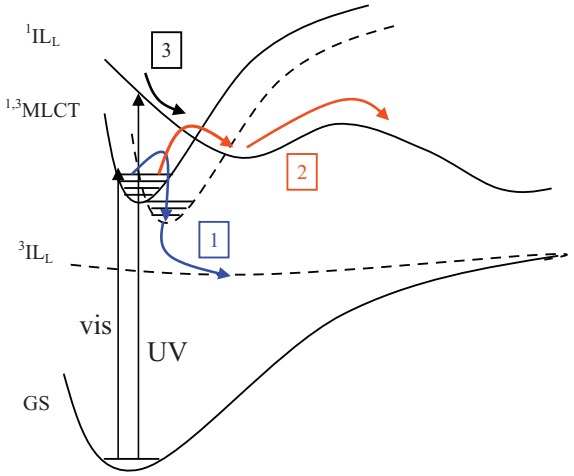

Scheme 2. Schematic view of the early elementary processes involved in the isomerization.

Upon irradiation in the visible energy domain and population of the ^{1}MLCT states localized on the bpy ligand, efficient ISC followed by intramolecular energy transfer will populate the low-lying ^3IL_L in the *trans* structure. The spin–orbit coupling between this state and the electronic ground state at the perpendicular geometry is nearly zero, explaining the long life-time (17 ns) found experimentally. Decay from the ^3IL_L to the ground state, *cis* or *trans*, is the last step of the isomerization process induced by visible light. Upon UV irradiation to the strongly absorbing ^1IL_L state an efficient transfer of population via a conical intersection to the $^1MLCT_{bpy}$ state around 35° occurs, and the ^{3}IL pathway of isomerization is activated again. This and the possibility of an ^{1}IL isomerization lead to a more efficient process.

With the help of our calculations and the available experimental data, we can attempt to extract key ingredients for the process under study. It appears that the photoisomerization of stilbene-like ligands coordinated to Re(I) polypyripyl complexes at UV/visible wavelengths is basically controlled, at the early stage, by three elementary processes: (i) the $^3MLCT \rightarrow {}^3IL$ transition due intramolecular energy transfer (which can also be viewed as an internal conversion between triplet states), (ii) the $^1MLCT \rightarrow {}^1IL$ internal conversion due to a conical intersection between these states, and (iii) the possible overcome of the energy barrier in the ^{1}IL state around a torsion angle of typically 60°. The efficiency and dynamics of these processes are very sensitive to the nature of the ligands, namely the isomerizable one and the π-acceptor one.

Three routes can be distinguished in Scheme 2. Route 1 is specific to visible light absorption around 400 nm, and proceeds only via the ^{1,3}MLCT and then ^{3}IL states. The energy gap between the ^{3}MLCT and ^{3}IL states will govern the time scale of the intramolecular energy transfer. Then isomerization proceeds on the ^{3}IL state, and the molecular system relaxes slowly to the *trans* or *cis* ground state geometry. Route 2 may occur at slightly higher excitation energies. Whether it can be activated or not will depend on the location of the conical intersection between ^{1}MLCT states and the ^{1}IL state. If the latter is sufficiently close to the MLCT states, population may be transferred from these states to the ^{1}IL state. Then isomerization can proceed in the ^{1}IL state, as in the free organic ligand. The relative energy of ^{1}MLCT and ^{1}IL states, as well as the height of the energy barrier in the ^{1}IL state, will govern the activation of this route. Note that if excitation of the ^{1}MLCT may open route 2 according to the criteria just discussed, it will actually open route 1 anyway.

The third route can occur after a direct excitation of the ^{1}IL state, in the UV domain. Here again, the height of the energy barrier will strongly influence the efficiency of this route. But, at least as important, is the conical intersection with the ^{1}MLCT states. Indeed, this conical intersection will allow for a very fast and efficient electronic population transfer to the ^{1}MLCT state, and open route 1 again. In fact, due to the presence of this conical intersection, route 1 will be most probably activated whatever the UV/visible excitation energy is.

Interestingly, in the experiment performed by Iha and coworkers [17,18], the isomerization quantum yields in the complexes with the bpe ligand are roughly constant for excitation energies from 400 to 313 nm. This suggests that route 2 or 3 is not activated. Even excited at 313 nm, where the ^{1}IL state absorbs, the quantum yield remains the same. The conical intersection will transfer the electronic population of the ^{1}IL state to ^{1}MLCT states and route 1 will be followed. For the complexes with stpy ligands [15,18], the isomerization quantum yield is increased at 365 nm excitation wavelength and above as compared to excitation at 400 nm. This suggests activation of route 2, since direct excitation in the ^{1}IL (at 330 nm) does not lead to a further increase in the quantum yield of isomerization.

In this contribution, we have presented theoretical results for the photoisomerization of stilbene-like ligands coordinated to Re(I) polypyripyl complexes. Our results are in accordance with experimental observations. We can draw several routes for isomerization, and shed light on the importance of the conical intersection between IL and MLCT states in the process. Varying the polypyridyl ligand in these complexes, as well as the study of dynamical and solvent effects will be the subject of further theoretical investigations.

Acknowledgments

This work was undertaken as part of the European collaborative-COST D35 and is supported by the Egide/DAAD Procope program (projects 20139VE and D/0811456). The calculations were carried out in part at the IDRIS and CINES computer centres (CNRS, Orsay, and Montpellier) through a grant of computer time from the Conseil Scientifique and at the LCQS (Strasbourg).

References

[1] A. Vlček Jr., M. Busby, Coord. Chem. Rev. 250 (2006) 1755.
[2] D.J. Stufkens, A. Vlček Jr., Coord. Chem. Rev. 177 (1998) 127.
[3] A. Vlček Jr., Top. Organomet. Chem. 29 (2010) 73.
[4] A. Kumar, S.-S. Sun, A.J. Lees, Coord. Chem. Rev., in this issue.
[5] W.K. Chan, Coord. Chem. Rev. 251 (2007) 2104.
[6] K.W. Cheng, W.K. Chan, Langmuir 21 (2005) 5247.
[7] K.D. Ley, C. Ed Whittle, M.D. Bartberger, K.S. Schanze, J. Am. Chem. Soc. 119 (1997) 3423.
[8] M. Zhang, P. Lu, X. Wang, L. He, H. Xia, W. Zhang, B. Yang, L. Liu, L. Yang, M. Yang, Y. Ma, J. Feng, D. Wang, N. Tamai, J. Photochem. Photobiol. B 108 (2004) 13185.
[9] A. Volker, H. Kunkely, Coord. Chem. Rev. 200–202 (2000) 991.
[10] V. Balzani, M. Venturi, A. Credi, Molecular Devices and Machines – A Journey into the Nano World, Wiley-VCH, Weinheim, 2003.
[11] V.W.-W. Yam, Y. Yang, J. Zhang, B.W.-K. Chu, N. Zhu, Organometallics 20 (2001) 4911.
[12] P.P. Zarnegar, C.R. Bock, D.G. Whitten, J. Am. Chem. Soc. 95 (1973) 4367.
[13] M.S. Wrighton, D.L. Morse, L. Pdungsap, J. Am. Chem. Soc. 97 (1975) 2073.
[14] M.S. Wrighton, D.S. Ginley, M.A. Schroeder, D.L. Morse, Pure Appl. Chem. 41 (1975) 671.
[15] M. Busby, P. Matousek, M. Towrie, A. Vlček Jr., J. Phys. Chem. A 109 (2005) 3000.
[16] O.S. Wenger, L.M. Henling, M.W. Day, J.R. Winkler, H.B. Gray, Inorg. Chem. 43 (2004) 2043.
[17] A.O.T. Patrocínio, N.Y.M. Iha, Inorg. Chem. 47 (2008) 10851.
[18] K.P.M. Frin, M.K. Itokazu, N.Y.M. Iha, Inorg. Chim. Acta 363 (2010) 294.
[19] L. Gagliardi, G. Orlandi, V. Molina, P.-Å. Malmqvist, B.O. Roos, J. Phys. Chem. A 106 (2002) 7355.
[20] J. Quenneville, T.J. Martínez, J. Phys. Chem. A 107 (2003) 829.
[21] L.M. Lawson Daku, J. Linares, M.-L. Boillot, Chem. Phys. Chem. 8 (2007) 1402.
[22] J. Bossert, C. Daniel, Chem. Eur. J. 12 (2006) 4835.
[23] S. Takeuchi, S. Ruhman, T. Tsuneda, M. Chiba, T. Taketsugu, T. Tahara, Science 322 (2008) 1073.

[24] D.H. Waldeck, Chem. Rev. 91 (1991) 415.
[25] E. Gindensperger, H. Köppel, C. Daniel, Chem. Commun. 46 (2010) 8225.
[26] D. Andrae, U. Häußermann, M. Dolg, H. Stoll, H. Preuß, Theor. Chim. Acta 77 (1990) 123.
[27] T.H. Dunning Jr., P.J. Hay, Methods of Electronic Structure Theory, Plenum Press, New York, 1977.
[28] P.-O. Widmark, P.-Å. Malmqvist, B.O. Roos, Theor. Chim. Acta 77 (1990) 291.
[29] B.O. Roos, R. Lindh, P.-Å. Malmqvist, V. Veryazov, P.-O. Widmark, J. Phys. Chem. A 108 (2005) 2851.
[30] B.O. Roos, R. Lindh, P.-Å. Malmqvist, V. Veryazov, P.-O. Widmark, J. Phys. Chem. A 109 (2005) 6575.
[31] K. Pierloot, B. Dumez, P.-O. Widmark, B.O. Roos, Theor. Chim. Acta 90 (1995) 87.
[32] M.J. Frisch, G.W. Trucks, H.B. Schlegel, G.E. Scuseria, M.A. Robb, J.R. Cheeseman, J.A. Montgomery Jr., T. Vreven, K.N. Kudin, J.C. Burant, J.M. Millam, S.S. Iyengar, J. Tomasi, V. Barone, B. Mennucci, M. Cossi, G. Scalmani, N. Rega, G.A. Petersson, H. Nakatsuji, M. Hada, M. Ehara, K. Toyota, R. Fukuda, J. Hasegawa, M. Ishida, T. Nakajima, Y. Honda, O. Kitao, H. Nakai, M. Klene, X. Li, J.E. Knox, H.P. Hratchian, J.B. Cross, C. Adamo, J. Jaramillo, R. Gomperts, R.E. Stratmann, O. Yazyev, A.J. Austin, R. Cammi, C. Pomelli, J.W. Ochterski, P.Y. Ayala, K. Morokuma, G.A. Voth, P. Salvador, J.J. Dannenberg, V.G. Zakrzewski, S. Dapprich, A.D. Daniels, M.C. Strain, O. Farkas, D.K. Malick, A.D. Rabuck, K. Raghavachari, J.B. Foresman, J.V. Ortiz, Q. Cui, A.G. Baboul, S. Clifford, J. Cioslowski, B.B. Stefanov, G. Liu, A. Liashenko, P. Piskorz, I. Komaromi, R.L. Martin, D.J. Fox, T. Keith, M.A. Al-Laham, C.Y. Peng, A. Nanayakkara, M. Challacombe, P.M.W. Gill, B. Johnson, W. Chen, M.W. Wong, C. Gonzalez, J.A. Pople, Gaussian 03, Gaussian, Inc., Wallingford, CT, 2004.
[33] K. Andersson, F. Aquilante, M. Barysz, E. Bednarz, A. Bernhardsson, M.R.A. Blomberg, Y. Carissan, D.L. Cooper, M. Cossi, A. Devarajan, L. De Vico, N. Ferré, M.P. Fülscher, A. Gaenko, L. Gagliardi, G. Ghigo, C. de Graaf, B.A. Hess, D. Hagberg, A. Holt, G. Karlström, J.W. Krogh, R. Lindh, P.-Å. Malmqvist, T. Nakajima, P. Neogrády, J. Olsen, T.B. Pedersen, J. Raab, M. Reiher, B.O. Roos, U. Ryde, B. Schimmelpfennig, M. Schütz, L. Seijo, L. Serrano-Andrés, P.E.M. Siegbahn, J. Stålring, T. Thorsteinsson, V. Veryazov, P.-O. Widmark, A. Wolf, MOLCAS, Version 7.2, Lund University Sweden, 2008.
[34] D.M. Dattelbaum, M.K. Itokazu, N.Y.M. Iha, T.J. Meyer, J. Phys. Chem. A 107 (2003) 4092.
[35] M.K. Itokazu, A.S. Polo, N.Y.M. Iha, J. Photochem. Photobiol. A 160 (2003) 27.
[36] W. Domcke, D.R. Yarkony, H. Köppel (Eds.), Conical Intersections: Electronic Structure, Dynamics and Spectroscopy, World Scientific, Singapore, 2004.